Kinetic model and Vlasov simulation verification of two-ion decay instability

D. J. Liu,[1] Qing Wang,[1] X. M. Li,[1] S. T. Zhang,[2] R. J. Cheng,[1] X. X. Li,[1] S. Y. Lv,[1] Z. M. Huang,[1] Qiang Wang,[1] Z. J. Liu,[1,3,*] L. H. Cao,[1,3] and C. Y. Zheng[1,3]

[1]*Institute of Applied Physics and Computational Mathematics, Beijing 100094, China*

[2]*HEDPS, Center for Applied Physics and Technology, and State Key Laboratory of Nuclear Physics and Technology, School of Physics, Peking University, Beijing 100871, China*

[3]*HEDPS, Center for Applied Physics and Technology, and College of Engineering, Peking University, Beijing 100871, China*

(Received 10 February 2023; accepted 27 July 2023; published 18 August 2023)

A kinetic theory is developed to describe the longitudinal decay of two-ion decay (TID): The pump ion-acoustic wave (IAW) decays into two daughter IAWs with a longer wavelength. The instability growth rate and threshold are given by the theory. Both the simulations of full kinetic Vlasov and hybrid Vlasov (kinetic ions and Boltzmann electrons) are employed to verify the theory and have a high quantitative agreement with the theory for $8 \leqslant ZT_e/T_i \leqslant 15$, where Z is the ion charge number and $T_i(T_e)$ is the ion (electron) temperature. The kinetic model developed here solves a long-standing problem that the simple fluid theory underestimates growth rate by a factor of $2 \sim 3$. Also, a reasonable explanation is given to the typical characteristics of TID that the dependence curves of subharmonic growth rate γ and wave number k.

DOI: 10.1103/PhysRevE.108.025206

I. INTRODUCTION

Ion acoustic waves (IAWs), as fundamental electrostatic waves in plasma, widely exist in astrophysics, space plasma, and fusion plasma. In inertial confinement fusion (ICF) experiments, laser light passes through the hohlraums, interacts with the plasma, and overlaps with multiple crossing laser beams. Understanding the control of the onset and saturation of stimulated Brillouin scattering (SBS) and crossed-beam energy transfer (CBET) mediated by IAWs is crucial to avoid laser energy loss and damage to expensive optical elements [1,2]. This decay of IAWs can act as an effective saturation mechanism for SBS and CBET, resulting in a crash in IAW amplitude that provokes a loss of plasma reflectivity.

Two-ion decay (TID) is a kind of parametric decay process [3,4], which is the decay of pump IAW into two daughter IAWs with longer wavelength. There are also several waves with similar linear dispersion relations shown in experiments and simulations to undergo decay to longer wavelength modes similarly, such as electron acoustic waves [5,6] and Trivelpiece-Gould waves [7–11]. The effect of TID on SBS saturation has been observed directly in Thomson scattering experiments [12–14]. Some numerical studies have also identified IAW decay during SBS saturation [15,16], e.g., a one-dimensional Vlasov simulation in Ref. [15] showed that the instantaneous SBS reflectivity saturates at ∼30% and drops to ∼0% due to TID. Also, some numerical work has studied IAW decay in isolation to avoid other effects that might interfere with the results [17–21], e.g., Ref. [17] showed a clear physical picture of the IAW decay into turbulence by one-dimensional (1D) Vlasov simulation.

Pesme *et al.* used seven-wave decay model in which the fundamental and the second-harmonic components of the IAW couple to a low-frequency daughter wave and to their Stokes and anti-Stokes satellites to study the stability of driven coherent IAW [22]. Three branches of instabilities (H1, H2, and modulation instability) were found to appear. The occurrence of each instability is discussed as a function of the frequency mismatch $\omega_{\rm mis} \equiv \omega_{\rm dri} - \omega_{\rm res}$, where $\omega_{\rm dri}$ is the driver frequency, $\omega_{\rm res}$ is the plasma response frequency. Both the H2 and modulation instability have the same scaling of $\gamma \propto {\varphi_m}^2$, while the H1 instability, also known as TID, has a scaling of $\gamma \propto \varphi_m$, where φ_m is the pump IAW amplitude. Therefore, in the small perturbation region ($\varphi \ll 1$) studied in this paper, TID is the dominant instability mechanism as long as TID can occur. H2 instability involves seven-wave coupling [22], modulation instability involves four-wave coupling [23]. While the H1 instability is a three-wave coupling process, and the three-wave model [17,18,24,25] is sufficient to describe it.

Through two-dimensional (2D) Vlasov simulation, Chapman *et al.* found that IAWs are susceptible to at least two distinct decay processes, the transversal decay channel of IAWs is still not clear so far, the longitudinal decay is known as TID, and the TID growth rate in 2D simulation is the same as the results obtained by the 1D system [19]. For IAW, the dispersion relation exhibits a near-linear behavior, whereby the wave vectors of three IAWs of TID parallel and pointed in the same direction due to three-wave matching. The resonant TID is prohibited in a strict sense in 1D cases. However, this process could be allowed when the dispersion spectrum is broadened. The existence of a finite amplitude pump wave can assess the frequency shift in a way that the resonance conditions are fulfilled, thus leading to TID [26]. Therefore, the TID theory typically focuses on longitudinal decay in one dimension [27].

*liuzj@iapcm.ac.cn

The fluid theories of TID were developed during the 1970s and 1980s (see Refs. [24,25]), and have attracted considerable attention in the last several decades. Where three-wave exact resonance was assumed, and the effect of harmonics was not taken into account. However, numerical studies have showed that the simple fluid model underestimate the growth rate by a factor of about $2 \sim 3$, and the threshold is often found to be overestimated by an order of magnitude [15,17,19]. Also, the simple fluid model cannot capture the independence of the subharmonic growth rate with the plasma parameters ZT_e/T_i, $k_0\lambda_{De}$ [17] (Z is the ion charge number, $T_e(T_i)$ is the electron (ion) thermal temperature, k_0 is the pump IAW wave number, and λ_{De} is the electron Debye length), which is vital for selecting the appropriate experimental parameters. Recently, an improved fluid model was proposed in Ref. [18] to describe TID, and the vortex-merging in ion phase space was found in the hybrid Vlasov simulation to result in a saturation of TID. Reference [28] considers the nonlinear frequency shift caused by superthermal electrons and finds it has a significant effect on the TID threshold and growth rate.

The fluid model, [17,24,25] which starts with the fluid equation of motion, cannot take into account the change in the distribution function, and thus cannot describe the effect of wave-particle interactions on instability. Although TID is a wave-wave interaction dominated process, wave-particle interactions also play an essential role in this instability. Strong evidence that trapped particles reduce the instability threshold below fluid models was provided by quantitative experiments on the parametric decay instability of Trivelpiece-Gould waves provided in Ref. [9]. In Ref. [20], the comparison of full and hybrid particle-in-cell simulation showed that the kinetic effect of electrons plays an essential role in the nonlinear evolution of a driven IAW, which will promote TID (only qualitative analysis is available), and saturate IAW at a low level. Therefore, it is necessary to develop a kinetic theory to further describe the TID.

In this paper, we developed a general kinetic model to describe the longitudinal decay of TID based on mode-mode coupling and multiple time-scale expansion. In the limit of zero detuning and damping, the growth rate is presented as $\gamma_0 = Q(v_p)\sqrt{k'k''}|\varphi_m|$. It is proportional to the pump IAW amplitude φ_m. And the TID has a maximum growth rate when both the wave number of the two daughter modes (k', k'') are half of the pump IAW wave number k_0. The coefficient $Q(v_p)$ reflects the coupling strength between the wave modes, is a function of phase velocity v_p, and dependent upon plasma parameters $k_0\lambda_{De}, ZT_e/T_i$. Both the fluid and kinetic theory based on mode-mode coupling have similar forms, and the differences are expressed in coefficient function $Q(v_p)$. It is a key quantity that determines the threshold and growth rate of TID. Comparing the theoretically predicted $Q(v_p)$ under different initial distribution conditions, it is found that the initial distribution function has a significant influence on the TID, which cannot be described by any fluid model.

Vlasov simulation under the parameter range $2.5 \leqslant ZT_e/T_i \leqslant 50$, $k_0\lambda_{De} = 0.3162$ is taken to validate our theory. Within the parameter range of $8 \leqslant ZT_e/T_i \leqslant 20$, the results of full kinetic simulation and hybrid simulation are consistent and highly consistent with our theory. Furthermore, the typical characteristics of TID that the dependence of subharmonic growth rate γ on wave number k takes the form of $|\sin(k\pi/k_0)|$ is explained by drawing on the wave-train model [11] of Trivelpiece-Gould waves.

The paper is organized as follows: In Sec. II, the kinetic model of TID is given, including the coupling equation between wave modes in Sec. II A, growth rate and threshold of TID in Sec. II B, and TID in the initial non-Maxwell case given in Sec. II C. The simulation setup and results are presented to verify the theory in Sec. III. Finally, some discussions and a summary are given in Secs. IV and V.

II. THEORETICAL ANALYSIS

A. Wave-wave coupling equations

Similar to the derivation of the decay instability of electron acoustic waves [7], we start with the one-dimensional Vlasov-Poisson equation instead of the fluid equations to capture the kinetic effect

$$\begin{aligned} \partial_t \mathrm{f}_s + v\partial_x \mathrm{f}_s - \frac{q_s}{m_s}\partial_x\varphi\partial_v \mathrm{f}_s = 0, \\ \partial_x^2\varphi = -4\pi\sum_{s=i,e} q_s \int \mathrm{f}_s dv, \end{aligned} \tag{1}$$

where f_s, q_s, m_s are the velocity distribution function, charge and mass of species s, s including electron and ion, φ is the electric potential. One can expand the distribution function and the potential into the Fourier series

$$\mathrm{f}_s(x, v, t) = n_{s0}\left(F_{s0}(v, t) + \sum_{m=-\infty}^{\infty}{}' \mathrm{f}_{s,m}(v, t)e^{ik_m x}\right), \tag{2}$$

$$\varphi = \sum_{m=-\infty}^{\infty}{}' \varphi_m(x, t)e^{ik_m x}, \tag{3}$$

where $\sum'$ denote that $m = 0$ is not included in the summation, n_{s0} is the initial unperturbed number density of species s, $f_{s,m}(v, t)$ is the mth Fourier component, satisfies $f_{s,-m}(v, t) = f^*_{s,m}(v, t)$. After substitution of Eqs. (2) and (3) into Eq. (1), one finds the Fourier components satisfy

$$\begin{aligned} &\partial_t \mathrm{f}_{s,m}(v, t) + ik_m v\mathrm{f}_{s,m}(v, t) - i\frac{q_s}{m_s}k_m\varphi_m(t)\partial_v F_{s,0}(v, t) \\ &= i\frac{q_s}{m_s}\sum_{m'=-\infty}^{\infty}(k_m - k_{m'})\varphi_{m-m'}(t)\partial_v \mathrm{f}_{s,m'}(v, t). \end{aligned} \tag{4}$$

The left-hand side of the above equation describes the linear oscillation of the perturbation mode, and the right-hand side of the equation is physical quantities that characterize the mode-mode coupling.

Assuming that the perturbation term $|f_{s,m}| \ll F_{s0}$, one can employ multiple time-scale expansion [29]

$$\begin{aligned} \mathrm{f}_{s,m}(v, t) &\simeq \varepsilon \mathrm{f}^{(1)}_{s,m}(v, \tau_0, \tau_1, \ldots) + \varepsilon^2 \mathrm{f}^{(2)}_{s,m}(v, \tau_0, \tau_1, \ldots) + \ldots \\ \varphi_m(t) &\simeq \varepsilon\varphi^{(1)}_m(\tau_0, \tau_1, \ldots) + \varepsilon^2\varphi^{(2)}_m(\tau_0, \tau_1, \ldots) + \ldots \\ F_{s0}(v, t) &\simeq F^{(0)}_{s0}(v, \tau_0, \tau_1, \ldots) + \varepsilon F^{(1)}_{s0}(v, \tau_0, \tau_1, \ldots) + \ldots, \end{aligned} \tag{5}$$

where $\varepsilon \ll 1$ is a small quantity that measures the magnitude of the perturbation. The time scales satisfy

$\partial_t\tau_0 = 1, \quad \partial_t\tau_1 = \varepsilon, \quad \partial_t\tau_2 = \varepsilon^2$. So the time derivative is expanded as $\partial_t = \partial_{\tau_0} + \varepsilon\partial_{\tau_1} + \varepsilon^2\partial_{\tau_2} + \ldots$. One can substitute Eq. (5) into Eq. (4), then separate each order of ε in those equations

$$\partial_{\tau_0} \mathrm{f}^{(1)}_{s,m}(v,\tau_0,\tau_1) + ivk_m \mathrm{f}^{(1)}_{s,m}(v,\tau_0,\tau_1) - \frac{iq_sk_m}{m_s}\varphi^{(1)}_m(\tau_0,\tau_1)\partial_v F^{(0)}_{s0}(v,\tau_0,\tau_1) = 0, \tag{6}$$

$$\partial_{\tau_0} \mathrm{f}^{(2)}_{s,m}(v,\tau_0,\tau_1) + \partial_{\tau_1} \mathrm{f}^{(1)}_{s,m}(v,\tau_0,\tau_1) + ik_m v \mathrm{f}^{(2)}_{s,m}(v,\tau_0,\tau_1) - \frac{iq_sk_m}{m_s}\varphi^{(2)}_m(\tau_0,\tau_1)\,\partial_v F^{(0)}_{s0}(v,\tau_0,\tau_1) = \frac{q_s i}{m_s}\sum_{m'=-\infty}^{\infty}(k_m - k_{m'})\varphi^{(1)}_{m-m'}(\tau_0,\tau_1)\partial_v \mathrm{f}^{(1)}_{m'}(v,\tau_0,\tau_1) + \frac{iq_sk_m}{m_s}\varphi^{(1)}_m(\tau_0,\tau_1)\partial_v F^{(1)}_{s0}(v,\tau_0,\tau_1), \tag{7}$$

$$\varphi^{(1)}_m(\tau_0,\tau_1) = k_m^{-2}4\pi\int\sum_s q_s n_{s0}\mathrm{f}^{(1)}_{s,m}(v,\tau_0,\tau_1)dv, \tag{8}$$

$$\varphi^{(2)}_m(\tau_0,\tau_1) = k_m^{-2}4\pi\int\sum_s q_s n_{s0}\mathrm{f}^{(2)}_{s,m}(v,\tau_0,\tau_1)dv, \tag{9}$$

$$\partial_{\tau_0} F^{(0)}_{s0}(v,\tau_0,\tau_1) = 0, \tag{10}$$

$$\partial_{\tau_1} F^{(0)}_{s0}(v,\tau_0,\tau_1) + \partial_{\tau_0} F^{(1)}_{s0}(v,\tau_0,\tau_1) = 0. \tag{11}$$

From Eqs. (10) and (11) one can obtain, $F^{(0)}_{s0} = F^0_{s0}(v,\tau_1)$ and $F^{(1)}_{s0}(v,\tau_0,\tau_1) = F^{(1)}_{s0}(v,\tau_0 = 0,\tau_1) - \tau_0\partial_{\tau_1}F^{(0)}_0(v,\tau_1)$. It can be seen that $\tau_0\partial_{\tau_1}F^{(0)}_0(v,\tau_1)$ is a small quantity compared to $F^{(1)}_{s0}(v,\tau_0,\tau_1)$. Therefore, we can consider that F^0_0 also does not vary on the slow time scale τ_1, $F^{(0)}_{s0}(v,\tau_0,\tau_1) = F^{(0)}_{s0}(v)$ is a constant.

Now we assume that the first-order potential and distribution oscillate in a fast time scale τ_0 with an amplitude varying slowly with τ_1:

$$\varphi^{(1)}_m(\tau_0,\tau_1) = \tfrac{1}{2}\varphi_m(\tau_1)e^{-i\omega_m\tau_0} + \text{c.c.} \tag{12}$$

$$\mathrm{f}^{(1)}_{s,m}(v,\tau_0,\tau_1) = \tfrac{1}{2}f_{s,m}(v,\tau_1)e^{-i\omega_m\tau_0} + \text{c.c.}, \tag{13}$$

where $\varphi^*_m(\tau_1) = \varphi_{-m}(\tau_1)$. According to the first-order Vlasov-Poisson [Eqs. (6) and (8)] the kinetic dispersion relation of IAW can be obtained as

$$D(\omega_m,k_m) = 1 - \sum_s\frac{\omega^2_{ps}}{k^2_m}\int dv\frac{\partial_v F^{(0)}_{s0}(v)}{v-\omega_m/k_m} = 0. \tag{14}$$

From the second-order Vlasov-Poisson equations, the wave-wave coupling equation (see Appendix A for details) can be obtained as

$$\frac{d}{dt}\varphi_m = -i\sum_{m'}N(m,m')\varphi_{m'}\varphi_{m''}e^{-i\Delta_{m,m'}t},$$

$$N(m,m') = \frac{k_{m'}}{2}\frac{\sum_s\frac{q_s}{m_s}\omega^2_{ps}\int\frac{\partial_v F^{(0)}_{s0}(v)}{(v-\omega_m/k_m)^3}dv}{\sum_s\omega^2_{ps}\int\frac{\partial_v F^{(0)}_{s0}(v)}{(v-\omega_m/k_m)^2}dv}, \tag{15}$$

where $m'' = m - m'$, $N(m,m')$ is the coupling coefficient measuring the strength of the decay from pumped IAW with wave number k_m to two daughter IAWs with wave number $k_{m'}$ and $k_{m''}$. Although the wave numbers are precisely matched ($k_m = k_{m'} + k_{m''}$), the frequencies are not always exactly matched in the actual simulation situation, $\Delta_{m,m'} \equiv \omega_m - \omega_{m'} - \omega_{m''}$ describes the amount of detuning among the three waves. $\omega_{ps} = \sqrt{4\pi n_s Z_s^2 e^2/m_s}$ is the species plasma frequency.

The coupling coefficient $N(m,m')$ determines the coupling strength, which is a key parameter affecting the TID growth rate and threshold (see Sec. II B). The calculation of the coupling coefficient requires the specification of the initial distribution function $F^{(0)}_{s0}(v)$.

With the initial Maxwellian distribution, $F^{(0)}_{s0}(v) = \frac{1}{v_{s,T}\sqrt{2\pi}}\exp(-v^2/2v^2_{s,T})$ ($v_{s,T} = \sqrt{T_s/m_s}$ is the thermal velocity of species s) the kinetic dispersion relation (Eq. (14)) can be reduced to

$$D(\omega_m,k_m) = 1 + \sum_s\chi_s, \tag{16}$$

where $\chi_s = \frac{W(b_s)}{(k\lambda_{Ds})^2}$ is the susceptibilities of species s, $b_s \equiv \omega_m/k_m v_{s,T}$, and $\mathrm{W}(b) = \frac{1}{\sqrt{2\pi}}\int\frac{xe^{-x^2/2}dx}{x-b}$ is the dispersion function [30].

For IAW in singer ion species, $b_e \ll 1$, $b_i \gg 1$, therefore $\mathrm{Re}[\chi_e] \approx \frac{1}{k^2\lambda^2_{De}}$, $\mathrm{Re}[\chi_i] \approx -\frac{\omega^2_{pi}}{\omega^2}(1 + \frac{3k^2v^2_{i,T}}{\omega^2})$. One can get the approximate form of the dispersion relation, which is just the same as the dispersion relation obtained from fluid theory

$$\frac{\omega_r}{k} = \sqrt{\frac{ZT_e}{m_i}}\sqrt{\frac{1}{1+k^2\lambda^2_{De}} + \frac{3T_i}{ZT_e}}. \tag{17}$$

Also, one can get the linear Landau damping Γ

$$\Gamma = \sqrt{\frac{\pi}{8}}\frac{\omega^3_r}{k^3v^3_{i,T}}\exp\left(-\frac{\omega^2_r}{2k^2v^2_{i,T}}\right). \tag{18}$$

It can also be obtained by numerically solving $D(\omega_K,k_m) = 0$, where $\mathrm{Re}[\omega_K]$, $\mathrm{Im}[\omega_K]$ is the kinetic frequency and damping of IAW.

Similarly, with the assumption of initial Maxwellian distribution, the coupling coefficient $N(m,m')$ in the wave-wave coupling equation Eq. (15) can be reduced to

$$N(m,m') = \frac{\frac{k_{m''}}{4}\sum_s\frac{q_s}{m_s}\frac{\omega^2_{ps}}{v^4_{s,T}}\left[\left(b_s{}^2-3\right)\mathrm{W}(b_s)+1\right]}{\sum_s\frac{\omega^2_{ps}}{v^3_{s,T}}([1-\mathrm{W}(b_s)]/b_s + b_s\mathrm{W}(b_s))}. \tag{19}$$

B. Growth rate and threshold

Assuming that only three IAWs (pump IAW m, two daughters IAW modes m', m'') are involved in the coupling process. The three IAWs satisfy $k_m = k_{m'} + k_{m''}$, and a minute frequency detuning $\Delta \equiv \omega_{m'} + \omega_{m''} - \omega_m$ usually exists in real situations. Then the TID coupling equation [Eq. (19)] can be

reduced to

$$\begin{aligned}\frac{d}{dt}\varphi_m &= -i\,\mathrm{N}(m,m')\varphi_{m'}\varphi_{m''}e^{i\Delta t},\\ \frac{d}{dt}\varphi_{m'} &= -i\,\mathrm{N}(m',m)\varphi_m\varphi^*_{m''}e^{-i\Delta t},\\ \frac{d}{dt}\varphi_{m''} &= -i\,\mathrm{N}(m'',m)\varphi_m\varphi^*_{m'}e^{-i\Delta t},\end{aligned} \tag{20}$$

where φ_m, φ'_m, φ''_m are the potential amplitudes of the pump and two daughter IAWs, respectively. In the weak dispersion region ($k_m\lambda_{De} \ll 1$), the three IAWs have the same phase velocity $\omega/k = v_p = \mathrm{Re}[\omega_K]/k$, approximately.

In the limit of exact matching of the three waves with zero detuning ($\Delta = 0$), the growth rate of the corresponding TID can be obtained as

$$\gamma_0 = \sqrt{N(m',m)N(m'',m)}|\varphi_m| = Q(v_p)\sqrt{k'k''}|\varphi_m|, \tag{21}$$

where coefficient $Q(v_p)$ is defined as

$$Q(v_p) = \left|\frac{\frac{1}{4}\sum_s \frac{q_s}{m_s}\frac{\omega_{ps}^2}{v_{s,T}^4}\left[\left(b_s^2-3\right)\mathrm{W}(b_s)+1\right]}{\sum_s \frac{\omega_{ps}^2}{v_{s,T}^3}\left([1-\mathrm{W}(b_s)]/b_s + b_s\mathrm{W}(b_s)\right)}\right|, \tag{22}$$

has the unit of velocity, is an important physical quantity reflecting the strength of mode-mode coupling.

Equation (21) clearly illustrates that the linear growth rate $\gamma_0 \propto \sqrt{k'k''}|\varphi_m|$, which is consistent with the fluid theory [17,18,24,25]. The difference between the final growth rate of the kinetic theory and the other fluid theories is only reflected in the coefficient function $Q(v_p)$. Figure 1 shows the function $Q(v_p)$ from different models varies with plasma parameters ZT_e/T_i and $k_0\lambda_{De}$. The coefficient function $Q(v_p)$ of fluid model in Ref. [17] is $v_p/2$, where $v_p = \sqrt{ZT_e/m_i}$ is the cold ion acoustic speed. The fluid model could explain why the most unstable wave modes during the TID process remain the wave mode with half of the fundamental mode wave number. But quantitatively, the fluid model significantly underestimates the growth rate of the simulation. Furthermore, $Q(v_p)$ in the fluid model keeps constant for different ZT_e/T_i, which is against the actual simulation.

In addition to the growth rate, the occurrence threshold is another quantity of interest to researchers on TID. From Eq. (20), one can get the threshold for the occurrence of TID by frequency detuning:

$$|\varphi_m|_{\mathrm{th}}^{\mathrm{detuning}} = \frac{|\Delta|}{2Q(v_p)\sqrt{k_{m'}k_{m''}}}. \tag{23}$$

If the nonlinear frequency shifts of IAWs (the shifts of three IAWs roughly cancel each other when evaluating Δ) are disregarded, the detuning is only brought on by weak IAW dispersion [17]. In the case where TID has maximum growth ($k_{m'} = k_{m''} = k_m/2$), from the fluid disperation Eq. (17), one can obtain $\Delta/\omega_m = -3/8k_m^2\lambda_{De}^2$, and TID threshold caused by frequency detuning $|\varphi_m|_{\mathrm{th}}^{\mathrm{detuning}} = \frac{3v_pk_m^2\lambda_{De}^2}{8Q(v_p)}$. It is scaled linearly with $k_m^2\lambda_{De}^2$, and inverse ratio with $Q(v_p)$. From Eq. (23), it is showed that the threshold is mainly influenced by $k_0\lambda_{De}$ and has little dependence on ZT_e/T_i. At parameter $k_0^2\lambda_{De}^2 = 0.1$, $Q(v_p) \approx 0.02$, Eq. (23) gives $|\varphi_m|_{\mathrm{th}}^{\mathrm{detuning}} \approx 0.05$ is greater than our simulation $|\varphi_m|_{\mathrm{th}}^{\mathrm{sim}} \approx 0.005$ for the reason that the actual detuning is smaller than the detuning from weak dispersion.

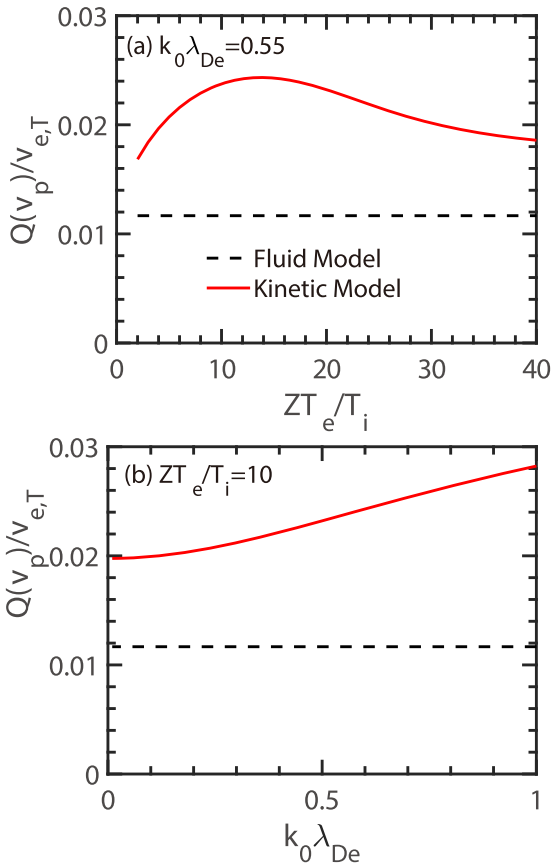

FIG. 1. Coefficient function $Q(v_p)$ as a function of ZT_e/T_i (a) and $k_0\lambda_{De}$ (b). The black dashed lines are the fluid model ($Q(v_p) = v_p/2$) in Ref. [17], and the red solid lines are the kinetic model [Eq. (22)].

The wave is damped by collision damping and collisionless Landau damping as it propagates. With the damping effect, the three-wave coupling equation becomes

$$\begin{aligned}\frac{d}{dt}\varphi_m + \Gamma_m\varphi_m &= -i\,\mathrm{N}(m,m')\varphi_{m'}\varphi_{m''}e^{i\Delta t},\\ \frac{d}{dt}\varphi_{m'} + \Gamma_{m'}\varphi_{m'} &= -i\,\mathrm{N}(m',m)\varphi_m\varphi^*_{m''}e^{-i\Delta t},\\ \frac{d}{dt}\varphi_{m''} + \Gamma_{m''}\varphi_{m'} &= -i\,\mathrm{N}(m'',m)\varphi_m\varphi^*_{m'}e^{-i\Delta t},\end{aligned} \tag{24}$$

where Γ_m, $\Gamma_{m'}$, $\Gamma_{m''}$ are the damping of pump IAW and two daughter IAWs, respectively. It can be approximated by the linear Landau damping [see Eq. (18)]. The threshold due to damping can be achieved as

$$|\varphi_m|_{\mathrm{th}}^{\mathrm{damp}} = \frac{\sqrt{\Gamma_{m'}\Gamma_{m''}}}{Q(v_p)\sqrt{k_{m'}k_{m''}}}. \tag{25}$$

In an actual simulation, the velocity distribution function is flattened by particle trapping after the pump IAW is excited, and the Landau damping is significantly lower than the initial value, $|\varphi_m|_{\mathrm{th}}^{\mathrm{damp}} \ll |\varphi_m|_{\mathrm{th}}^{\mathrm{detuning}}$.

For the most unstable case, $k_{m'} = k_{m''} = k_m/2$, and two daughter IAW have the same damping rate $\Gamma_{m'} = \Gamma_{m''} = \Gamma$, then one can obtain the growth rate after considering both damping and detuning:

$$\gamma = \sqrt{k_m^2 Q^2(v_p)|\varphi_m|^2/4 - \Delta^2/4} - \Gamma, \tag{26}$$

and the total threshold for the occurrence of TID

$$|\varphi_m|_{\text{th}}^{\text{tol}} = \frac{2}{Q(v_p)k_m}\sqrt{\Gamma^2 + \frac{\Delta^2}{4}}. \tag{27}$$

C. TID in the initial non-Maxwellian distribution

It is well known that when a particle system is at thermal equilibrium, the particles follow the Maxwellian velocity distribution. However, in actual physical processes, plasmas are rarely in equilibrium. For example, in the laser fusion experiment, excited waves trap particles, forming a plateau or even a bump near the phase velocity [31]. In space plasma, there are more high-velocity particles than there should be if the space plasma are in equilibrium. The kappa distribution is widely used to describe the distribution [32]. For the laser-irradiated plasma in ICF, inverse bremsstrahlung is the dominant heating mechanism. In 1980, Landon [33] predicted that super-Gaussian distributions would be produced in plasmas heated by inverse bremsstrahlung absorption of sufficiently strong electromagnetic radiation, which is called the Landon effect [34–37].

Therefore, it is necessary to discuss the evolution of TID coefficients when plasmas are in non-Maxwellian distribution. To simplify the coefficient functions $Q(v_p)$, we introduce the generalized Z function

$$Z_s(\zeta_s, \bar{F}_{s0}(z)) = \int_{-\infty}^{+\infty} \frac{\bar{F}_{s0}(z)}{z - \zeta_s} dz, \tag{28}$$

where z, ζ_s, $\bar{F}_{s0}(z)$ are normalized speed, phase velocity ω_m/k_m and the initial velocity distribution function with $\sqrt{2}v_{s,T}$ as the normalized unit. According to the definition of the generalized Z function, one can get the following equation:

$$\begin{aligned}
&\int_{-\infty}^{+\infty} \frac{\partial_v F_{s0}(v)}{(v - v_p)^n} dv \\
&= \frac{1}{(\sqrt{2}v_{s,T})^{n+1}} \int_{-\infty}^{+\infty} \frac{\partial_z \bar{F}_{s0}(z)}{(z - \zeta_s)^n} dz \\
&= \frac{1}{(n-1)!} \frac{1}{(\sqrt{2}v_{s,T})^{n+1}} \frac{\partial^n Z_s(\zeta_s, \bar{F}_{s0}(z))}{\partial^n \zeta_s}; \quad n \geqslant 1.
\end{aligned} \tag{29}$$

With the above equation, the theoretical formulation of TID under any initial distribution can be written in an elegant form by the generalized Z function. Then the dispersion relationship of IAW can be reduced to

$$D(\omega_m, k_m) = 1 - \sum_s \frac{1}{k^2 \lambda_{Ds}^2} \frac{1}{2} \frac{\partial Z_s(\zeta_s, \bar{F}_{s0})}{\partial \zeta_s}, \tag{30}$$

and the coefficient function $Q(v_p)$ can be represented as

$$\mathrm{Q}(v_p) = \frac{1}{2}\left| \frac{\sum_s \frac{q_s}{m_s}\omega_{ps}^2 \frac{1}{8v_{s,T}^4} Z'''_s(\zeta_s, \bar{F}_{s0}(z))}{\sum_s \omega_{ps}^2 \frac{1}{(\sqrt{2}v_{s,T})^3} Z''_s(\zeta_s, \bar{F}_{s0}(z))} \right|. \tag{31}$$

Once the initial distribution function is given, the frequency of IAW, coefficient function $Q(v_p)$, TID growth rate and threshold can be obtained by Eqs. (30), (31), and (26), (27), respectively.

In the case of the initial Maxwellian distribution, $\bar{F}_{s0} = \bar{F}_M = e^{-z^2}/\sqrt{\pi}$, one can obtain

$$\begin{aligned}
Z'_s(\zeta_s, \bar{F}_M(z)) &= -2W(b_s = \sqrt{2}\zeta_s), \\
Z''_s(\zeta_s, \bar{F}_M(z)) &= -2\sqrt{2}\partial_{b_s} W(b_s) \\
&= 2\sqrt{2}([(1 - W(b_s)]/b_s + b_s W(b_s)), \\
Z'''_s(\zeta_s, \bar{F}_M(z)) &= -4\partial_{b_s}^2 W(b_s) \\
&= -4[({b_s}^2 - 3)W(b_s) + 1].
\end{aligned} \tag{32}$$

It is easy to verify that the generalized coefficient function Eq. (31) is consistent with the previous result Eq. (22).

One may find that the generalized Z function is a Hilbert transform of the velocity distribution function. Therefore, we can calculate the nth-order derivative of the Z function by calculating the Hilbert transform of the nth-order derivative of the distribution function

$$\frac{\partial^n Z_s(\zeta_s, \bar{F}_{s0}(z))}{\partial^n \zeta_s} = \int_{-\infty}^{+\infty} \frac{\partial_z^n \bar{F}_{s0}(z)}{z - \zeta_s} dz. \tag{33}$$

With the generalized Z function solver in Ref. [38], one can numerically obtain the IAW frequency and the TID coefficient function $Q(v_p)$ on a given arbitrary initial distribution.

To investigate the effect of the change in the initial distribution function on the TID, we set both electrons and ions in hydrogen plasma to be one-dimensional kappa distribution [39]:

$$F_\kappa(v) = \frac{1}{\sqrt{\pi\kappa\theta_{s,T}^2}} \frac{\Gamma(\kappa)}{\Gamma(\kappa - 1/2)} \left[1 + \frac{1}{\kappa}\frac{v^2}{\theta_{s,T}^2}\right]^{-\kappa}, \tag{34}$$

where $\theta_{s,T} = \sqrt{\frac{2(\kappa-3/2)}{\kappa}} v_{s,T}$ is the most probable speed, $\Gamma(z) = \int_0^{+\infty} t^{z-1} e^{-t} \mathrm{d}t$ is the Gamma function. The kappa distribution converges to the Maxwellian distribution when the kappa index κ goes to infinity. And the kappa index κ, has to be larger than $3/2$ to make sure the convergence of the second moment of the kappa distribution. The normalized distribution function (normalized with $\sqrt{2}v_{s,T}$) used to calculate the generalized Z function is $\bar{F}_\kappa(z) = \frac{1}{\sqrt{\pi(\kappa-3/2)}} \frac{\Gamma(\kappa)}{\Gamma(\kappa-1/2)} [1 + \frac{z^2}{\kappa-3/2}]^{-\kappa}$.

Figure 2 shows the IAW frequency and the TID coefficient function $G(v_p)$ under different κ. It is shown that the initial distribution function has a significant influence on the TID, which cannot be described by fluid model. The more low-energy particles (with larger κ), the higher the frequency of IAW. And, the increase in the number of low-energy electrons suppresses TID when $ZT_e/T_i < 6$, and promotes TID when $ZT_e/T_i > 6$.

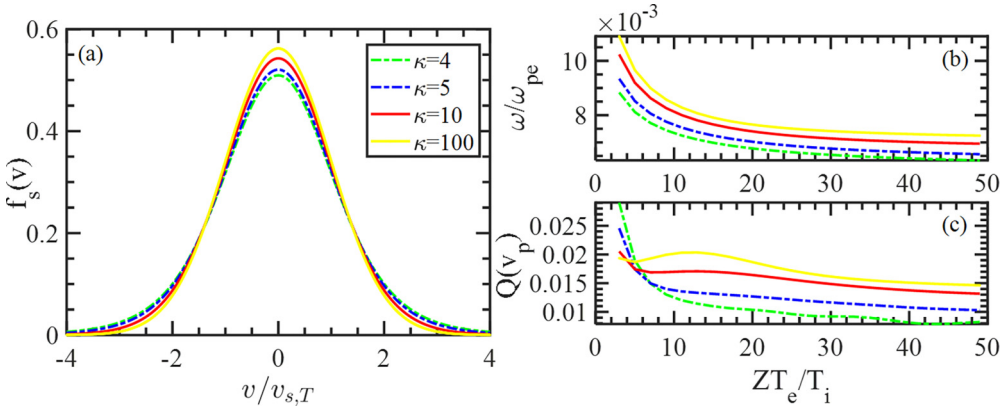

FIG. 2. (a) The kappa distribution with different κ. (b) Frequency of IAW and (c) $Q(v_p)$ as a function of ZT_e/T_i, when $k_0\lambda_{De} = 0.3162$.

III. VLASOV SIMULATION

A. Simulation setup

The Vlasov method is well known for being free of statistical noise and enabling clear simulation for ion phase space. Therefore, we used the 1D Vlasov code VLAMA to study TID in hydrogen plasma. The code has two versions of the solver, hybrid Vlasov solver [18] and full Vlasov solver [30,40–45]. When there is no laser field, the only difference between the two solvers is how the electron density n_e is calculated. For the full-Vlasov solver, $n_e = \int f_e(x, v)\mathrm{d}v$, where f_e is the velocity distribution of electrons. For the hybrid-Vlasov solver, electrons are described by Boltzmann distribution: [46,47] $n_e = n_{e0}\exp[e(\varphi + \varphi_d)/T_e]$, where n_{e0} is the initial equilibrium density, φ is the electrostatic potential related to the plasma and $\varphi_d(t, x) = \varphi_d(t)\cos[k_0(x - v_p^d t)]$ is external electrostatic potential acting as a driver. The phase velocity of driving potential v_p^d is chosen from the fluid dispersion Eq. (17) to excite pump IAWs with wave number $k_0 = 0.3162\lambda_{De}^{-1}$.

The same part of the two solvers is shown as follows. The motion of ion species i is described by Vlasov-Poisson equations

$$\frac{\partial f_i}{\partial t} + v\frac{\partial f_i}{\partial x} - \frac{q_i\nabla(\varphi + \varphi_d)}{m_i}\frac{\partial f_i}{\partial v} = 0, \tag{35a}$$

$$\frac{\partial^2\varphi}{\partial x^2} = -4\pi e(n_i - n_e), \tag{35b}$$

where f_i is ion velocity distribution function for species i initialized with the Maxwellian distribution, q_i, m_i, are ion charge and ion mass. The density of kinetic ions is obtained by $n_i = \int f_i(x, v)\mathrm{d}v$. The external potential is given by $\frac{\phi_d(t)}{\phi_{d0}} = \frac{1}{2}[\tanh(R(\frac{2t}{t_{\mathrm{ramp}}} - 1)) - \tanh(R(\frac{2(t - t_{\mathrm{stop}})}{t_{\mathrm{ramp}}} - 1))]$, where $R = 4$, $t_{\mathrm{stop}}\omega_{pe} = 4 \times 10^4$, $t_{\mathrm{ramp}}\omega_{pe} = 500$. To solve the Vlasov equation, Eq. (35a), the Vlasov equation can be split into two advection equations

$$\frac{\partial f_i}{\partial t} - \frac{q_i\nabla(\varphi + \varphi_d)}{m_i}\frac{\partial f_i}{\partial v} = 0, \tag{36a}$$

$$\frac{\partial f_i}{\partial t} + v_i\frac{\partial f_i}{\partial x} = 0. \tag{36b}$$

Then, a third-order Van Leer scheme [48] is used to solve the advection equations. In space, we have imposed periodic boundary conditions, and a Fourier transform-based routine has been used to solve the Poisson equation.

The phase space domain is $[0, L] \times [-v_{\max}, v_{\max}]$, where the system length $L = 8 \times 2\pi/k_0$ for hybrid simulation, and $L = 2 \times 2\pi/k_0$ for full-Vlasov simulation. It has been verified that the spatial scale has little influence on the rate of TID growth when $L \geqslant 2 \times \pi/k_0$. The cut-off velocity $v_{\max}$ is selected to be large enough to ensure that the integral of the distribution function is n_i, which was usually taken as $8v_{i,T}$, and a bigger value when T_i is small. The size of spatial grids $N_x = 64 \times 8$ for hybrid Vlasov simulation, $N_x = 64 \times 2$ for full Vlasov simulation, and the grids of velocity $N_v = 2 \times 512 + 1$, the time step $\mathrm{dt} = 0.05\omega_{pe}^{-1}$ for both the hybrid and full Vlasov simulation. The driving amplitude $e\phi_{d0}/T_e$ varies from 10^{-4} to 10^{-1} to excite IAW of different amplitudes.

B. Simulation results

Figure 3 shows the TID process during the nonlinear evolution of IAW with plasma parameters $ZT_e/T_i = 8$, $k_0\lambda_{De} = 0.3162$, $Zm_e/m_i = 1/1836$, $L = 8 \times 2\pi/k_0$. For more details, see our previous work Ref. [18] and the references [17,19,49,50] therein. The evolution of IAWs can be divided into three stages: stage I ($0 < t\omega_{pe} < 4 \times 10^4$), Resonantly excitation of ion acoustic wave; stage II ($4 \times 10^4 < t\omega_{pe} < 1.5 \times 10^5$), the slow subharmonics growth; stage III ($1.5 \times 10^5 < t\omega_{pe}$), system evolution into turbulence.

In stage I, a driver of strength $e\varphi_d/T_e = 0.01$ is applied to resonantly exciting IAW for a duration of $4 \times 10^4\omega_{pe}^{-1}$, the frequency of excited pump IAW $\omega_{sim} = 8.22 \times 10^{-3}\omega_{pe}$, which is near the kinetic frequency $\mathrm{Re}[\omega_K] = 8.35 \times 10^{-3}\omega_{pe}$, and slightly above the fluid theory predicted the frequency $\omega_F = 7.87 \times 10^{-3}\omega_{pe}$. The wave number in the system is mainly the fundamental mode ($k = k_0$) and its second harmonic until stage III [see Figs. 3(a) and 3(b)].

In stage II, after the driver is switched off, the electric field amplitude remains approximately constant, and the average amplitude $\langle e\lambda_{De}E/T_e\rangle_\tau$ over the time interval τ, is 2.6×10^{-2}. The subharmonic modes (wave number $k \neq nk_0$, $n = 1, 2, 3...$) grow slowly exponentially due to the TID process [see Fig. 3(d)] from the round-off errors [51] (about 2.2×10^{-16}), and the growth rate was obtained by fit in the time interval τ. The fitting time interval τ throughout this

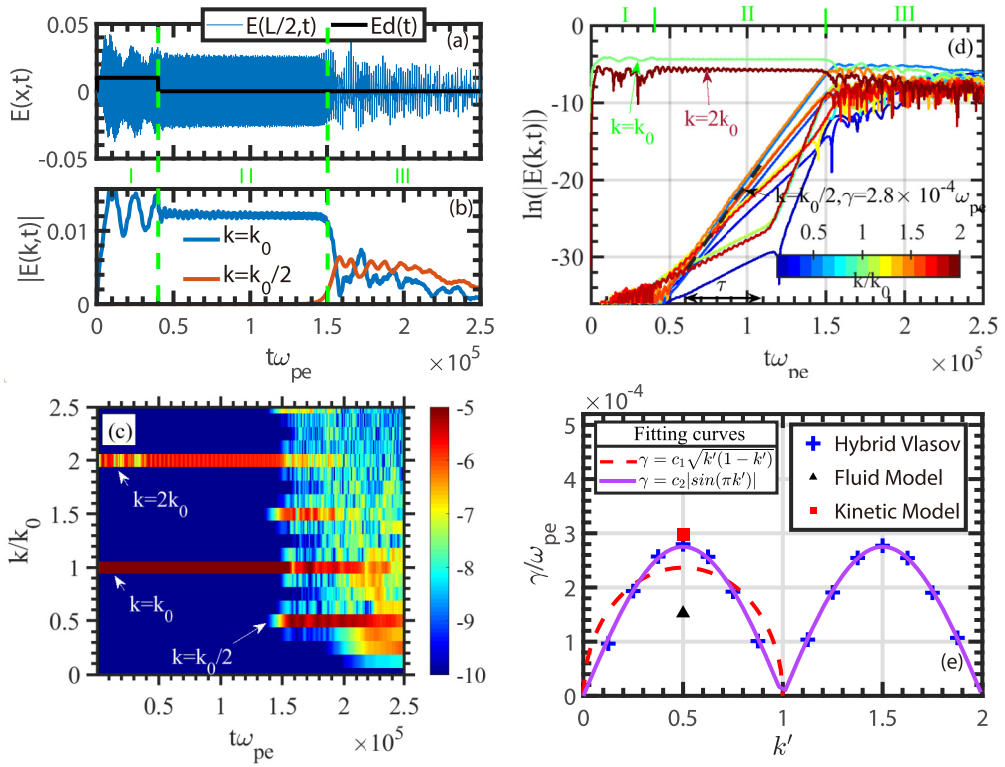

FIG. 3. IAW undergoing two-ion decay with parameters $ZT_e/T_i = 8$, $k_0\lambda_{De} = 0.3162$, $Zm_e/m_i = 1/1836$, $L = 8 \times 2\pi/k_0$, $\langle e\lambda_{De}E/T_e\rangle_\tau \approx 2.6 \times 10^{-2}$ by hybrid Vlasov simulation. (a) Evolution of the electric field, and $E_d(t)$ is the amplitude of external driving electric field. (b) Evolution of the wave modes with wave number $k = k_0/2, k_0$. (c), (d) Evolution of the wave modes $\ln(|E(k,t)|)$. (e) Growth rate of all wave number in the range $0 < k < 2k_0$. The blue crosses (labeled as Hybrid Vlasov) are the growth rates obtained by fitting in Fig. 3(d) over the time interval $\tau \in [6 \times 10^4, 1.2 \times 10^5]\omega_{pe}^{-1}$, the black triangle, red square are the maximum TID growth rates of Fluid and Kinetic model, respectively. The red dotted line and purple solid line are fitting curves of two different theoretical models with $c_1 = 4.73 \times 10^{-4}$, $c_2 = 2.75 \times 10^{-4}$, $k' = k/k_0$.

article was selected in the initial linear growth stage, and $\tau \in [6 \times 10^4, 1.2 \times 10^5]\omega_{pe}^{-1}$ for the parameters of Fig. 3.

When the power of the daughter and the pumping IAWs are comparable, phase vortex merging occurs, [18] and then the evolution of IAW enters stage III. As shown in Fig. 3(c), the wave number spectral gradually transitions from discrete to continuous, and the system eventually evolves into turbulence.

The comparison of simulation results and theoretical prediction of maximum growth rate is shown in Fig. 3(d). The kinetic model in this paper can get better prediction results compared with the fluid model in Ref. [17]. The fluid model can only describe the wave-wave interaction, while the kinetic model can consider the effect of the change of distribution function on TID, as a result, can describe the weak wave-particle interaction and wave-wave interaction. In addition, the effect of ion thermal pressure on TID is not taken into account in the fluid model. Therefore, the kinetic model can give a more accurate prediction.

Another interesting phenomenon shown in Fig. 3(d) is that the growth rate as a function of k looks like a periodic arch-bridge, is maximal at and symmetric about $k = (n - 1/2)k_0$, $n = 1, 2, 3\ldots$, and is periodic in k_0. This is a characteristic feature of TID [15,17–19]. The periodic behavior has not been adequately explained yet. From the previous section, it is shown that $\gamma \propto \sqrt{k'(1-k')}$, $k' = k/k_0$ in both the kinetic theory of this paper and the previous fluid theory. It does not fit the simulation results well and does not explain the growth of subharmonic with wave number greater than k_0 either.

In Ref. [8], a new parametric instability mechanism caused by weakly trapped particles in the potential wells of a wave train was first put forward to describe the decay of Trivelpiece-Gould waves. Later, the same group further validated and enriched this theory in experimental simulations [9–11]. Their work was focused on Trivelpiece-Gould waves, but the idea of their theory can also be used qualitatively to explain the properties of waves with similar linear dispersion relations, such as IAWs discussed in this article.

In this parametric instability, peaks in the wave potential move with respect to one another, some peaks move closer, and others move away from each other. The motion is replicated along the wave train, creating a periodic structure which is the growing daughter, the schematic diagram is shown in Fig. 4. The model takes potential peaks initially at equally spaced positions $s_n = n\lambda_0$, where λ_0 is the wavelength of pump IAW. Between each peaks, there are trapped particles with a uniform phase space density. Then the peaks suffered some slight disturbance, slowly varying from their initial position by a small amount δs_n. The trapped particles reflect from peaks, and apply a force to the nth peaks $\delta F_n = \beta(\delta s_{n+1} - 2\delta s_n + \delta s_{n-1})$, β can be thought of a coefficient of negative compressibility for trapped particles. Besides, the peak n also suffers a repulsion force $\delta F_{Rn} =$

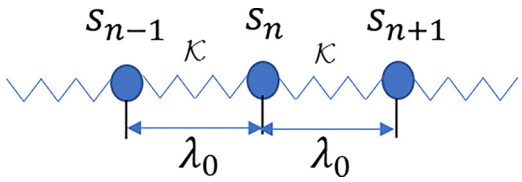

FIG. 4. Schematic of the wave train. The blue balls represent wave peaks, the spring in the middle describes the restoring force between the wave packets, $\mathcal{K}$ is the "spring constant". s_n is the position of nth wave peak, and the initial distance between wave packets is $\lambda_0 = 2\pi/k_0$.

$-\mathcal{K}[(\delta s_n - \delta s_{n-1}) - (\delta s_{n+1} - \delta s_n)]$ from the adjacent peaks, $\mathcal{K}$ is the "spring constant". Then the Newton's law

$$\mathcal{M}\delta\ddot{s}_n = \delta F_n + \delta F_{Rn} \tag{37}$$

can be employed to calculate the movement of the nth peak, where $\mathcal{M}$ is the inertial mass of the nth peak. The values of $\beta, \mathcal{K}, \mathcal{M}$ of Trivelpiece-Gould waves can be obtained following the way of Refs. [8,11]. Assuming the perturbation satisfaction form $\delta s_n \propto \exp(iks_n - i\omega t)$, which is consistent with Floquet's theorem [52], then one can obtain the dispersion relations

$$\omega^2 = 4\frac{\mathcal{K}-\beta}{\mathcal{M}}\sin^2(k\pi/k_0). \tag{38}$$

The instability occurs when the destabilizing negative compressibility β of weak trapped particle overcome the repulsive spring constant $\mathcal{K}$. Then the growth rate of this instability can be obtained as

$$\gamma = \sqrt{\frac{2(\beta-\mathcal{K})}{\mathcal{M}}}|\sin(k'\pi)|, \tag{39}$$

where $k' = k/k_0$ is the normalized wave vector.

As shown in Fig. 3(e), the typical characteristic of TID, the curve of γ-k during the TID process can be perfectly described by this instability. First, the periodic arch-bridge growth rate curve is fitted by the above equation very well. Besides, the instability growth rate peaks at $k = n \times k_0/2$ and is independent of the parameters ZT_e/T_i, $k_0\lambda_{De}$, as well as IAW amplitude is also predicted by the above equation.

To further verify the correctness of our theory and test the parameter space to which the theory applies, we simulate the TID process in different ZT_e/T_i by both full kinetic and hybrid kinetic Vlasov solver. Figure 5 shows the results with parameters $k_0\lambda_{De} = 0.3162$, $ZT_e/T_i = 10, 11, 15, 20$. In such medium ZT_e/T_i parameter region, the results of the hybrid Vlasov solver are close to those of the full kinetic Vlasov solver, suggesting that the effect of electron kinetics on the TID coupling coefficient is not significant, and hybrid simulation is sufficient to describe the TID process. When the amplitude of the driven ion acoustic wave is not large (linear parameter region), there is a linear dependence between the

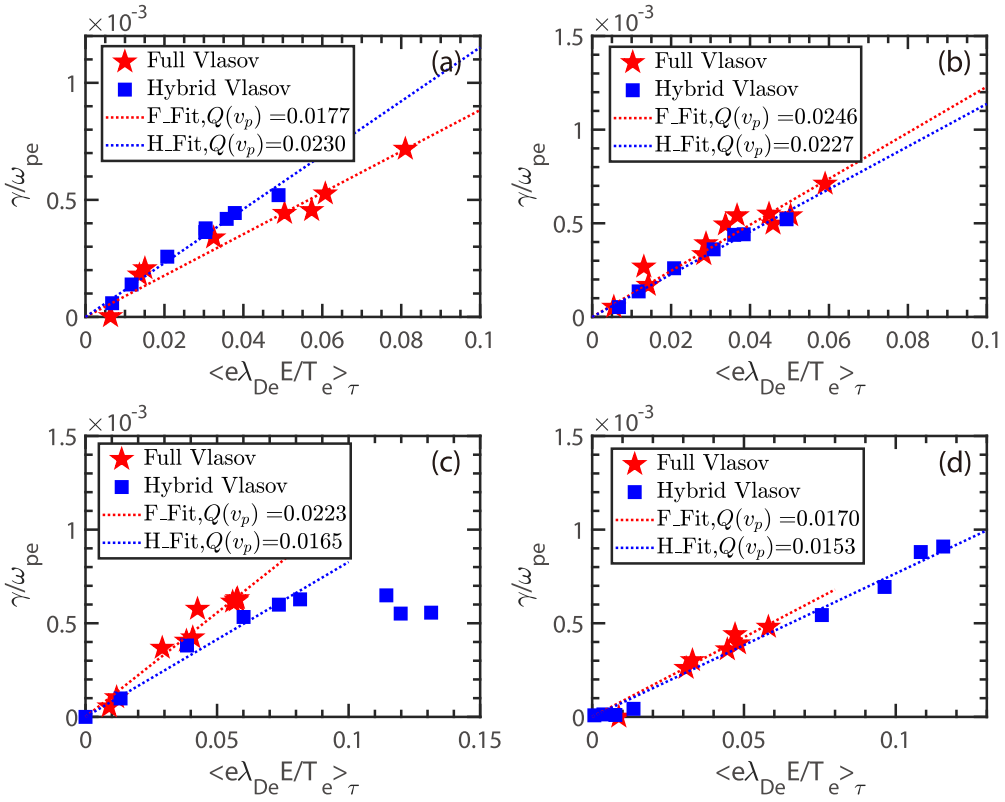

FIG. 5. The scaling of $\gamma_{\max}$ with average electric field amplitude $\langle e\lambda_{De}E/T_e\rangle_\tau$ with parameters $k_0\lambda_{De} = 0.3162$, (a) $ZT_e/T_i = 10$, (b) $ZT_e/T_i = 11$, (c) $ZT_e/T_i = 15$, (d) $ZT_e/T_i = 20$. The red stars and blue diamonds are the growth rate of full Vlasov and hybrid Vlasov simulations; the red and blue lines are the fitting line, and TID coefficient function $Q(v_p)$ is obtained from the slope of the fitting lines and Eq. [21].

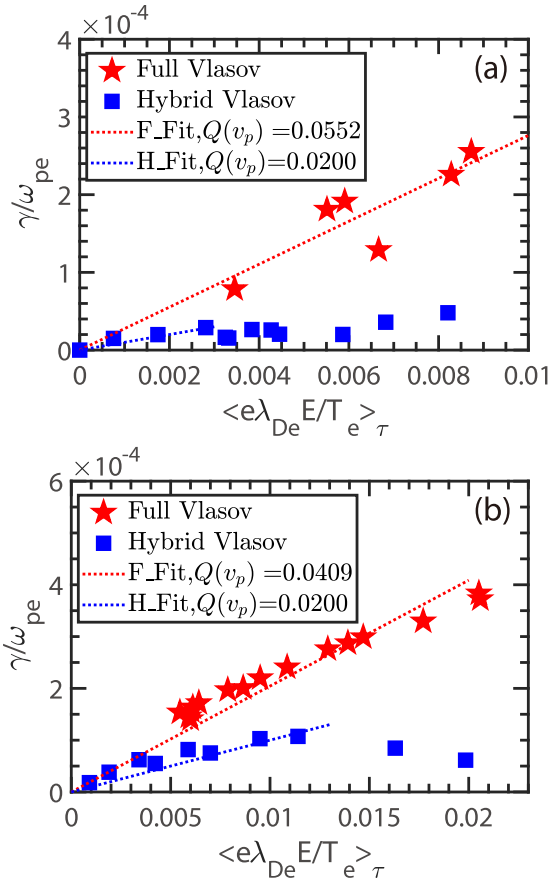

FIG. 6. The scaling of $\gamma_{\max}$ with average electric field amplitude $\langle e\lambda_{De}E/T_e\rangle_\tau$ with parameters $k_0\lambda_{De} = 0.3162$, with small ZT_e/T_i: (a) $ZT_e/T_i = 2.5$, (b) $ZT_e/T_i = 5$.

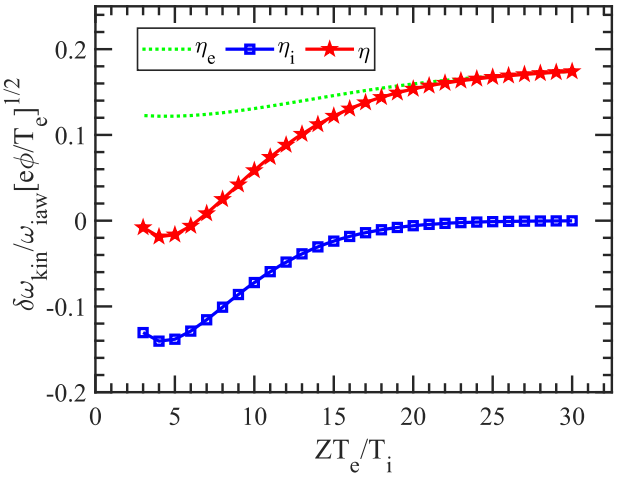

FIG. 7. Kinetic nonlinear frequency shift assuming adiabatic wave excitation for all species for $k\lambda_{De} = 0.3162$.

growth rate and IAWs amplitude, which is consistent with our theory. When the amplitude of IAW is larger than a threshold (nonlinear parameter region), the growth rate gradually saturates and no longer increases with E, as shown in Fig. 5(c). The threshold E_{th} can be estimated by setting the trapping width $2\sqrt{\frac{q_i E_{\text{th}}}{k_0 m_i}}$ equal to the phase velocity v_p. This yields E_{th} approximately equals to $k_0/4 \approx 0.08$, which is close to the simulation.

In the case of large ZT_e/T_i, such as $ZT_e/T_i = 30, 50$, the phase velocity v_p is much greater than $v_{i,T}$, a wide plateau near the phase velocity is easily formed due to particle trapping, thereby the distribution function deviates substantially from the Maxwell distribution near the phase velocity. The analytic expressions of the coefficient functions $Q(v_p)$ with initial platform distribution is shown to be dependent on trapped width which is related to the amplitude of IAWs. Therefore, the growth rate is no longer scaled linearly with the IAW amplitude. It is verified by our Vlasov simulation, the result is not shown here, for similar results are available in Ref. [17].

In the case of small ZT_e/T_i (such as $ZT_e/T_i = 2.5, 5$), the result is shown in Fig. 6. It can be observed that the γ scaled linearly with E holds only in very small IAW amplitude, which suggests that TID is weak and not such important at these parameters. The reason is explained as follows.

According to Pesme's fluid seven-wave theory, [22] the driven IAW has three distinct branches instabilities (H2, modulation instability and TID), each with its corresponding frequency mismatch range. For TID, it has a cutoff mismatch $\delta\omega_{co}/\omega_{\text{iaw}} \sim 3k_m^2\lambda_{De}^2/8 + e\varphi_m/T_e$. When the frequency mismatch $\delta\omega_{\text{mis}}/\omega_m$ is greater than the cut-off mismatch $\delta\omega_{co}/\omega_{\text{iaw}}$, TID cannot occur. In our simulation, the driver frequency ω_{dri} is chosen from the plasma linear fluid dispersion relation ω_{flu}, which is close to the numerical solution of kinetic dispersion relation ω_{kin}, the plasma response frequency ω_{res} can be modeled by nonlinear frequency shift $\delta\omega_{\text{kin}}$. Then we have $\omega_{\text{res}} = \omega_{\text{kin}} + \delta\omega_{\text{kin}}$, $\omega_{\text{dri}} = \omega_{\text{flu}} \approx \omega_{\text{kin}}$, therefore the frequency mismatch can be obtained by kinetic nonlinear frequency shift $\omega_{\text{mis}} = \omega_{\text{dri}} - \omega_{\text{res}} \approx -\delta\omega_{\text{kin}}$. The kinetic nonlinear frequency shift $\delta\omega_{\text{kin}}$ can be modeled by the expression $\delta\omega_{\text{kin}} = \eta\omega_{\text{iaw}}(e\phi_m/T_e)^{1/2}$. The parameter η, can be decomposed as $\eta = \eta_i + \eta_e$, where η_i and η_e corresponding the contributions of ions and electrons, which can be obtained by Eq. (4) in Ref. [53]. Figure 7 shows the kinetic nonlinear frequency shift parameter η of all species. The contribution of electrons to the kinetic frequency shift is always positive, and the parameter η_e slowly increases from 0.12 to 0.17 as ZT_e/T_i increases. The contribution of ions to the kinetic frequency shift is always negative, and the parameter η_i gradually increases from -0.14 to near zero as ZT_e/T_i increases. The total frequency shift parameter η change from a negative value to close to η_e.

At small ZT_e/T_i region ($ZT_e/T_i \leqslant 5$), both η_i and η_e are negative, $\delta\omega_{\text{mis}} = -\delta\omega_{\text{kin}} = -\eta(e\varphi_m/T_e)^{1/2}$ is positive, and the IAW amplitude that can undergo TID is greatly limited by the condition $\delta\omega_{\text{mis}} < \delta\omega_{co}$, therefore TID growth rate is greatly weaker than the result of the medium ZT_e/T_i parameter ($5 < ZT_e/T_i \leqslant 20$); Besides, because $|\eta_i| > |\eta|$ when $ZT_e/T_i \leqslant 5$, the IAW amplitude allowed by TID in Hybrid-Vlasov simulation is lower than that in the full-Vlasov simulation. All of this aforementioned phenmena are in high qualitative agreement with our simulation results (see Figs. 5 and 6).

Figure 8 and Table I show the comparison of theoretical and simulation results of the coefficient function of TID.

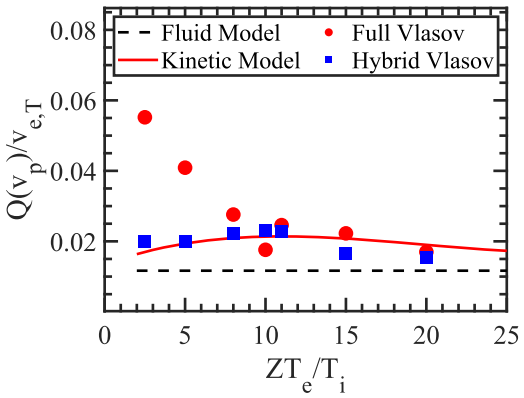

FIG. 8. Comparison of theoretical and simulation results of the coefficient function TID.

As we can see, $Q(v_p)$ of the simple fluid model does not change with ZT_e/T_i, and underestimated the simulation results at medium ZT_e/T_i region. In Ref. [17], a similar result, scaling of maximum growth rate of subharmonic (The corresponding wave number $k = k_0/2$) with ZT_e/T_i, in the parameter $\langle|e\varphi/T_e|\rangle_\tau \sim 0.1$ is shown. It should be noted that when $ZT_e/T_i > 20$, the maximum growth rate $\gamma_{\max}$ is no longer proportional to $\langle|e\varphi/T_e|\rangle_\tau$ (explained in Sec. II B), and in the case of $ZT_e/T_i < 8$, $\langle|e\varphi/T_e|\rangle_\tau \sim 0.1$ is beyond the linear growth region of $\gamma_{\max}$ versus $|e\varphi/T_e|$. Therefore, the $Q(v_p)$ obtained from the fitting could describe the characteristics of TID better. In medium ZT_e/T_i region ($8 \leqslant ZT_e/T_i \leqslant 20$), the kinetic model have a high level of agreement with the simulation results. In large ZT_e/T_i region ($ZT_e/T_i > 20$), $Q(v_p)$ is related with IAW amplitude. Hence, it is not shown here. In small ZT_e/T_i region, TID is very weak. due to large frequency mismatch $\delta\omega_{\text{mis}}$ limits the IAW amplitude that can undergo TID.

Although TID is weak and of less significance when ZT_e/T_i is small, it cannot be denied that there are still some unclear physics within this parameter interval: the $Q(v_p)$ obtained by the full Vlasov simulation and hybrid simulation differ somewhat, and there is also a deviation from theories. Here, we give some possible speculative guesses qualitatively. I. As it can be seen in Fig. 6, the hybrid-Vlasov simulation result does not maintain good linearity, and the Q value obtained by linear fitting is highly dependent on the selection of fitting interval; II. Under this parameter, the TID growth rate is small, some other instabilities, such as H2 instability and modulation instability may play an important role, resulting in the Q obtained from simulation fitting being larger than our theory. III. The IAW dispersion relation is near-linear and the initial amplitude of TID's daughter wave is small, the corresponding nonlinear frequency shift can be ignored. Therefore, the frequency shift of the pump wave $\delta\omega_{\text{kin}}$ approximately equal to the frequency detuning Δ of Eq. (20). According to Eq. (26) and Ref. [28], when the frequency detuning Δ is comparable to the TID growth rate, it can significantly suppress or even prevent TID. Under low ZT_e/T_i parameters, and $|\delta\omega_{\text{kin}}|$ in hybrid simulations is larger than full Vlasov simulation, it will cause the growth rate of hybrid simulations to be lower than that of full kinetic simulations; At medium ZT_e/T_i region ($8 <= ZT_e/T_i <= 20$), a large frequency shift requires a large fundamental amplitude, but at this time the TID growth rate itself is very large. Therefore, although the kinetic effect of electrons causes differences between η_i and η, it has little effect on TID growth rate.

IV. DISCUSSION

Although the kinetic model is successful with moderate ZT_e/T_i parameters and finite amplitude pumping waves. It should be noted that all theories have their applicable parameter range. The fluid models can only describe wave-wave interaction. Our kinetic model can describe wave-wave interaction and weak wave-particle interaction, but can hardly deal with strong wave-particle interactions. The derivation of the kinetic model assumes (I) that the detuning is much smaller than the pump wave frequency $\Delta_{m,m'} \ll \omega_m$, (II) that all trapping effects can be described perturbatively, thereby, the theory can only describe TID of finite amplitude IAW, (III) harmonics of the pump IAW are weak, and do not participate in the decay process.

In both the fluid and kinetic models, the growth rate is scaled linearly with pump IAW amplitude. Theoretically, changes in the plasma parameters (such as ZT_e/T_i, $k_0\lambda_{De}$) will only affect the coupling coefficients $Q(v_p)$ and will not affect the linear dependence of γ and φ.

However, in some extreme parameter space, $\gamma \propto \varphi^n$, $n \neq 1$ can be observed. For instance, when the pump IAW is very strong, the detuning $\Delta_{m,m'} \ll \omega_m$ is invalid, thereby, the kinetic model is no longer applicable and the growth rate will no longer satisfy $\gamma \propto \varphi_m$. Also, when $ZT_e/T_i > 20$, the growth rate is shown to scale with a higher power of φ_m. In that case, a wide plateau near the phase velocity is easy to form, and the wave-particle interaction is such strong that all the weak turbulence theories cannot describe the simulation results. Besides, if the harmonics of pump IAW are strong

TABLE I. Summary of theoretical and simulation results of the coefficient function $Q(v_p)$. Here, $v_p = \sqrt{ZT_e/m_i}$, $\text{Re}[\omega_K]/k$ is used to calculate theoretical $Q(v_p)$ for fluid model and Kinetic model, respectively.

	ZT_e/T_i	2.5	5	8	10	11	15	20
$Q(v_p)$ of Vlasov simulation	Full Vlasov	0.0552	0.0409	0.0276	0.0177	0.0246	0.0223	0.0170
	Hybrid Vlasov	0.0200	0.0200	0.0222	0.0230	0.0227	0.0165	0.0153
$Q(v_p)$ of two models	Fluid Model	0.0117	0.0117	0.0117	0.0117	0.0117	0.0117	0.0117
	Kinetic Model	0.0170	0.0194	0.0209	0.0213	0.0214	0.0208	0.0190
v_p used in two models	Fluid Model	0.0233	0.0233	0.0233	0.0233	0.0233	0.0233	0.0233
	Kinetic Model	0.0364	0.0307	0.0278	0.0267	0.0263	0.0251	0.0243

enough to participate in the decay, it may suppress the instability according to the multiwave version of fluid three-wave parametric resonance theory of Trivelpiece-Gould waves [54]. In addition, if the daughter IAW intensity is close to the pump IAW, the power of the daughter IAWs cannot be ignored when calculating the TID growth rate (Eq. [21]). There is an extreme case that the daughter IAW mode is not growing anymore when its intensity is the same as pump IAW mode, which leads to $n < 1$.

V. SUMMARY

In this paper, a kinetic model has been developed to predict the decay of IAW. Both full kinetic Vlasov and hybrid Vlasov simulations were taken to verify this theory. For $8 \leqslant ZT_e/T_i \leqslant 15$, the predictions of this model can be well matched to both full kinetic Vlasov and hybrid Vlasov simulation. In addition, this model is extended to describe TID in the case of arbitrary initial distribution with the help of the generalized Z function. The comparison of the results by the initial distribution at different κ shows that the initial distribution function has a significant impact on the TID, which cannot be adequately described by any fluid model. Besides, we find the TID growth rate curve γ-k formed as $|\sin(k\pi/k_0)|$ for the first time. We have established the results in a collisionless 1D plasma, and multidimensional and collisional effects remain to be investigated.

The data that support the findings of this study are available from the corresponding author upon reasonable request.

ACKNOWLEDGMENTS

This work was supported by the National Natural Science Foundation of China (Grants No. 11975059, No. 12005021, No. 11875241 and No. 11875091).

The authors declare no competing financial interest.

APPENDIX A: DERIVATION OF THE COUPLING EQUATION

To derivation of the coupling equation, one can substitute the first-order equation Eqs. (12) and (13) into Eq. (7), then obtain

$$\begin{aligned}
&\partial_{\tau_0} \mathrm{f}^{(2)}_{s,m}(v,\tau_0,\tau_1) + \frac{1}{2}\frac{q_s}{m_s}\partial_{\tau_1}\left[\frac{\varphi_m(\tau_1)\partial_v F^{(0)}_{s,0}(v)}{v-\omega_m/k_m}e^{-i\omega_m\tau_0} + \frac{\varphi_{-m}(\tau_1)\partial_v F^{(0)}_{s,0}(v)}{v+\omega^*_m/k_m}e^{i\omega^*_m\tau_0}\right] \\
&\quad + ik_m v\mathrm{f}^{(2)}_{s,m}(v,\tau_0,\tau_1) - \frac{ik_m q_s}{m_s}\varphi^{(2)}_m(\tau_0,\tau_1)\partial_v F^{(0)}_{s,0}(v) \\
&\quad = \frac{iq_s^2}{2m_s^2}\sum_{m'=-\infty}^{\infty}(k_m - k_{m'})\varphi^{(1)}_{m-m'}(\tau_0,\tau_1)\partial_v\left[\frac{\varphi_{m'}(\tau_1)\partial_v F^{(0)}_{s,0}(v)}{v-\omega_{m'}/k_{m'}}e^{-i\omega_{m'}\tau_0} + \frac{\varphi_{-m'}(\tau_1)\partial_v F^{(0)}_{s,0}(v)}{v+\omega^*_{m'}/k_{m'}}e^{i\omega^*_{m'}\tau_0}\right].
\end{aligned} \tag{A1}$$

The expression $\partial_v F^{(1)}_0(v,\tau_0,\tau_1) = 0$ is used to obtain the above equation. For the parameter region we are interested in, the detuning is smaller compared to the frequency of IAWs, $(\omega_{m'} + \omega_{m''} - \omega_m) \ll \omega_m$. Thus, we can define the detuning Δ as

$$\omega_{m'} + \omega_{m''} - \omega_m = \varepsilon\Delta, \quad \tau_0(\omega_{m'} + \omega_{m''} - \omega_m) = \varepsilon\tau_0\Delta = \tau_1\Delta. \tag{A2}$$

With the above definitions and Eq. (12), one can further simplify Eq. (A1) as

$$\begin{aligned}
&\partial_{\tau_0} \mathrm{f}^{(2)}_{s,m}(v,\tau_0,\tau_1) + ik_m v\mathrm{f}^{(2)}_{s,m}(v,\tau_0,\tau_1) - \frac{ik_m q_s}{m_s}\varphi^{(2)}_m(\tau_0,\tau_1)\partial_v F^{(0)}_{s,0}(v) \\
&\quad = -\frac{1}{2}\frac{q_s}{m_s}\partial_{\tau_1}\left[\frac{\varphi_m(\tau_1)\partial_v F^{(0)}_{s,0}(v)}{v-\omega_m/k_m}e^{-i\omega_m\tau_0} + \frac{\varphi_{-m}(\tau_1)\partial_v F^{(0)}_{s,0}(v)}{v+\omega^*_m/k_m}e^{i\omega^*_m\tau_0}\right] \\
&\qquad + \frac{iq_s^2}{4m_s^2}\sum_{m'=-\infty}^{\infty} k_{m''}\varphi_{m''}\varphi_{m'}\partial_v\left[\frac{\partial_v F^{(0)}_{s,0}(v)}{v-\omega_{m'}/k_{m'}}\right]e^{-i\omega_m\tau_0 - i\Delta\tau_1} + \frac{iq_s^2}{4m_s^2}\sum_{m'=-\infty}^{\infty} k_{m''}\varphi^*_{m''}\varphi_{m'}\partial_v\left[\frac{\partial_v F^{(0)}_{s,0}(v)}{v-\omega_{m'}/k_{m'}}\right]e^{-i(\omega_{m'}-\omega^*_{m''})\tau_0} \\
&\qquad + \frac{iq_s^2}{4m_s^2}\sum_{m'=-\infty}^{\infty} k_{m''}\varphi^*_{m''}\varphi_{m'}\partial_v\left[\frac{\partial_v F^{(0)}_{s,0}(v)}{v-\omega_{m'}/k_{m'}}\right]e^{-i(\omega_{m'}-\omega^*_{m''})\tau_0} + \frac{iq_s^2}{4m_s^2}\sum_{m'=-\infty}^{\infty} k_{m''}\varphi_{m''}\varphi^*_{m'}\partial_v\left[\frac{\partial_v F^{(0)}_{s,0}(v)}{v+\omega^*_{m'}/k_{m'}}\right]e^{i(\omega^*_{m'}-\omega_{m''})\tau_0} \\
&\qquad + \frac{iq_s^2}{4m_s^2}\sum_{m'=-\infty}^{\infty} k_{m''}\varphi^*_{m''}\varphi^*_{m'}\partial_v\left[\frac{\partial_v F^{(0)}_{s,0}(v)}{v+\omega^*_{m'}/k_{m'}}\right]e^{i\omega^*_m\tau_0 + i\Delta^*\tau_1},
\end{aligned} \tag{A3}$$

where $k_{m''} = k_m - k_{m'}$. Then one can perform a Laplace transform on Eqs. (A3) and (9) for fast time variable τ_0 by

$$\hat{f}^{(2)}_k(p,\tau_1) = \int_0^\infty d\tau_0 f^{(2)}_k(\tau_0,\tau_1)e^{-p\tau_0}, \quad f^{(2)}_k(\tau_0,\tau_1) = \frac{1}{2\pi i}\int_C d\tau_0 \hat{f}^{(2)}_k(p,\tau_1)e^{p\tau_0}. \tag{A4}$$

Choosing a suitable time τ_0 as the starting moments to make sure $\mathrm{f}_m^{(2)}(v,\tau_0=0,\tau_1)=0$, then from Eq. (A3), one can get

$$
\begin{aligned}
&(p+ik_m v)\hat{\mathrm{f}}_{s,m}^{(2)}(p)-\frac{iq_s k_m}{m_s}\hat{\varphi}_m^{(2)}(p)\partial_v F_{s0}^{(0)}\\
&=-\frac{q_s}{2m_s}\frac{1}{p+i\omega_m}\frac{\partial_{\tau_1}\varphi_m(\tau_1)\partial_v F_{s0}^{(0)}}{v-\omega_m/k_m}-\frac{q_s}{2m_s}\frac{1}{p-i\omega_m^*}\frac{\partial_{\tau_1}\varphi_m^*(\tau_1)\partial_v F_{s0}^{(0)}}{v+\omega_m^*/k_m}\\
&\quad+\frac{i}{4}\frac{q_s^2}{m_s^2}\sum_{m'=-\infty}\varphi_{m'}\varphi_{m''}\partial_v\left[\frac{k_{m''}\partial_v F_{s0}^{(0)}}{v-\omega_{m'}/k_{m'}}\right]\frac{e^{-\Delta\tau_1}}{p+i\omega_m}+\frac{i}{4}\frac{q_s^2}{m_s^2}\sum_{m'=-\infty}\varphi_{m'}\varphi_{m''}^*\partial_v\left[\frac{k_{m''}\partial_v F_{s0}^{(0)}}{v+\omega_{m'}^*/k_{m'}^*}\right]\frac{1}{p+i\omega_{m'}-i\omega_{m''}^*}\\
&\quad+\frac{i}{4}\frac{q_s^2}{m_s^2}\sum_{m'=-\infty}\varphi_{m'}^*\varphi_{m''}\partial_v\left[\frac{k_{m''}\partial_v F_{s0}^{(0)}}{v+\omega_{m'}^*/k_{m'}^*}\right]\frac{1}{p-i\omega_{m'}^*+i\omega_{m''}}+\frac{i}{4}\frac{q_s^2}{m_s^2}\sum_{m'=-\infty}\varphi_{m'}^*\varphi_{m''}^*\partial_v\left[\frac{k_{m''}\partial_v F_{s0}^{(0)}}{v+\omega_{m'}^*/k_{m'}^*}\right]\frac{e^{\Delta^*\tau_1}}{p-i\omega_m^*}.
\end{aligned}
\tag{A5}
$$

Performing the Laplace transform on the second-order Poisson equation, Eq. (9), one can obtain

$$
\hat{\varphi}_m^{(2)}(p,\tau_1)=k_m^{-2}4\pi\int\sum_s q_s n_{s0}\hat{\mathrm{f}}_{s,m}^{(2)}(v,p,\tau_1)dv. \tag{A6}
$$

Substitute Eq. (A5) into Eq. (A6), using Eq. (14) to simplify the result, then obtain

$$
\begin{aligned}
\hat{\varphi}_m^{(2)}(p,\tau_1)=&\frac{k_m^{-2}}{D(p,k_m)}\int\sum_s\left[\frac{\omega_{ps}^2 dv}{p+ik_m v}-\frac{1}{2}\frac{1}{p+i\omega_m}\frac{\partial_{\tau_1}\varphi_m(\tau_1)\partial_v F_{s0}^{(0)}}{v-\omega_m/k_m}-\frac{1}{2}\frac{1}{p-i\omega_m^*}\frac{\partial_{\tau_1}\varphi_m^*(\tau_1)\partial_v F_{s0}^{(0)}}{v+\omega_m^*/k_m}\right.\\
&+\frac{i}{4}\frac{q_s}{m_s}\sum_{m'=-\infty}\varphi_{m'}\varphi_{m''}\partial_v\left[\frac{k_{m''}\partial_v F_{s0}^{(0)}}{v-\omega_{m'}/k_{m'}}\right]\frac{e^{-\Delta\tau_1}}{p+i\omega_m}+\frac{i}{4}\frac{q_s}{m_s}\sum_{m'=-\infty}\varphi_{m'}\varphi_{m''}^*\partial_v\left[\frac{k_{m''}\partial_v F_{s0}^{(0)}}{v+\omega_{m'}^*/k_{m'}^*}\right]\frac{1}{p+i\omega_{m'}-i\omega_{m''}^*}\\
&\left.+\frac{i}{4}\frac{q_s}{m_s}\sum_{m'=-\infty}\varphi_{m'}^*\varphi_{m''}\partial_v\left[\frac{k_{m''}\partial_v F_{s0}^{(0)}}{v+\omega_{m'}^*/k_{m'}^*}\right]\frac{1}{p-i\omega_{m'}^*+i\omega_{m''}}+\frac{i}{4}\frac{q_s}{m_s}\sum_{m'=-\infty}\varphi_{m'}^*\varphi_{m''}^*\partial_v\left[\frac{k_{m''}\partial_v F_{s0}^{(0)}}{v+\omega_{m'}^*/k_{m'}^*}\right]\frac{e^{\Delta^*\tau_1}}{p-i\omega_m^*}\right].
\end{aligned}
\tag{A7}
$$

The inverse Laplace transform back to time space is then required. The results include secular and nonsecular terms (grow in an unbounded way). On the right-hand side (RHS) of the above equation, the first, second, third, and sixth terms of the inverse Laplace transform are secular, while the fourth and fifth terms of the transform are nonsecular. The complex conjugate of the inverse Laplace transform results of the first and third terms, is the second and sixth terms of the RHS of Eq. (A7), respectively. The inverse Laplace transform on the first terms on the RHS of the Eq. (A7) is given by

$$
\begin{aligned}
&L\left\{\frac{-k_m^{-2}}{D(\omega_m,k_m)}\int\sum_s\left[\frac{\omega_{ps}^2 dv}{p+ik_m v}\frac{1}{2}\frac{1}{p+i\omega_m}\frac{\partial_{\tau_1}\varphi_m(\tau_1)\partial_v F_{s0}^{(0)}}{v-\omega_m/k_m}\right\}\right.\\
&=-k_m^{-2}\sum_s\int dv\frac{\omega_{ps}^2\partial_{\tau_1}\varphi_m(\tau_1)\partial_v F_{s0}^{(0)}}{v-\omega_m/k_m}\frac{1}{2}\int_C\frac{dp/(2\pi i)}{p+ik_m v}\frac{e^{p\tau_0}}{D(p,k_m)(p+i\omega_m)}\\
&\simeq-k_m^{-2}\sum_s\int dv\frac{\omega_{ps}^2\partial_{\tau_1}\varphi_m(\tau_1)\partial_v F_{s0}^{(0)}}{v-\omega_m/k_m}\frac{1}{2}\int_C\frac{dp/(2\pi i)}{p+ik_m v}\frac{e^{p\tau_0}}{\partial_p D(p,k_m)\big|_{p=-i\omega_m}(p+i\omega_m)^2}\\
&=-k_m^{-2}\sum_s\int dv\frac{\omega_{ps}^2\partial_{\tau_1}\varphi_m(\tau_1)\partial_v F_{s0}^{(0)}}{v-\omega_m/k_m}\frac{1}{2}\frac{i\tau_0 e^{-i\omega_m\tau_0}}{k_m(v-\omega_m/k_m)\partial_p D(p,k_m)\big|_{p=-i\omega_m}}\\
&=\frac{1}{2}\tau_0 e^{-i\omega_m\tau_0}\partial_{\tau_1}\varphi_m(\tau_1)\sum_s\left[\frac{ik_m^{-2}\omega_{ps}^2}{\partial_p D(p,k_m)\big|_{p=-i\omega_m}}\int dv\frac{\partial_v F_{s0}^{(0)}}{k_m(v-\omega_m/k_m)^2}\right]\\
&=-\frac{1}{2}\tau_0 e^{-i\omega_m\tau_0}\partial_{\tau_1}\varphi_m.
\end{aligned}
\tag{A8}
$$

The above equation is obtained by only keeping the secular term with the approximate relationship given below

$$\begin{aligned}\int_C \frac{e^{p\tau_0}/(2\pi i)}{(p+ik_m v)(p+i\omega_m)D(p,k_m)}dp &= \int_C \frac{e^{p\tau_0}/(2\pi i)}{(p+ik_m v)(p+i\omega_m)^2\partial_p D(p,k_m)|_{p=-i\omega_m}}ds \\ &= -\frac{e^{-ik_m v\tau_0}}{(\omega_m-k_m v)^2\partial_p D(p,k_m)|_{p=-i\omega_m}} + \frac{e^{-i\omega_m\tau_0}}{(\omega_m-k_m v)^2\partial_p D(p,k_m)|_{p=-i\omega_m}} \\ &\quad - \frac{i\tau_0 e^{-i\omega_m\tau_0}}{(k_m v-\omega_m)\partial_p D(p,k_m)|_{p=-i\omega_m}} \\ &\approx -\frac{i\tau_0 e^{-i\omega_m\tau_0}}{(k_m v-\omega_m)\partial_p D(p,k_m)|_{p=-i\omega_m}}. \end{aligned} \tag{A9}$$

Using a similar approach, the inverse Laplace transform on the third terms of RHS of Eq. (A7) can be obtained as

$$\begin{aligned} & L\left\{\frac{k_m^{-2}}{D(p,k_m)}\int\sum_s\left[\frac{\omega_{ps}^2 dv}{p+ik_m v}\frac{i}{4}\frac{q_s}{m_s}\sum_{m'=-\infty}\varphi_{m'}\varphi_{m''}\partial_v\left[\frac{k_{m''}\partial_v F_{s0}^{(0)}}{v-\omega_{m'}/k_{m'}}\right]\frac{e^{-\Delta\tau_1}}{p+i\omega_m}\right]\right\} \\ &= k_m^{-2}\frac{i}{4}\sum_{m'=-\infty}\varphi_{m'}\varphi_{m''}e^{-\Delta\tau_1}\int dv\sum_s\left[\frac{q_s}{m_s}\omega_{ps}^2 k_{m''}\partial_v\left[\frac{\partial_v F_{s0}^{(0)}}{v-\omega_{m'}/k_{m'}}\right]\int\frac{e^{p\tau_0}/(2\pi i)dp}{D(p,k_m)(p+ik_m v)(p+i\omega_m)}\right] \\ &= k_m^{-2}\frac{i}{4}\sum_{m'=-\infty}\varphi_{m'}\varphi_{m''}e^{-\Delta\tau_1}\int dv\sum_s\left[\frac{q_s}{m_s}\omega_{ps}^2 k_{m''}\partial_v\left[\frac{\partial_v F_{s0}^{(0)}}{v-\omega_{m'}/k_{m'}}\right]\frac{-i\tau_0 e^{-i\omega_m\tau_0}}{\partial_p D(p,k_m)|_{p=-i\omega_m}(k_m v-\omega_m)}\right] \\ &= \frac{1}{4}\tau_0 e^{-i\omega_m\tau_0}\sum_{m'=-\infty}\varphi_{m'}\varphi_{m''}e^{-\Delta\tau_1}\int dv\sum_s\left[\frac{q_s}{m_s}\omega_{ps}^2 k_{m''}\partial_v\left[\frac{\partial_v F_{s0}^{(0)}}{v-\omega_{m'}/k_{m'}}\right]\frac{dv}{(k_m v-\omega_m)}\frac{1}{k_m^2\partial_p D(p,k_m)|_{p=-i\omega_m}}. \end{aligned} \tag{A10}$$

For the sake of removing the secular terms from RHS of Eq. (A7), the following equations must be satisfied:

$$\begin{aligned} &\frac{d}{dt}\varphi_m = -i\sum_{m'}N(m,m')\varphi_{m'}\varphi_{m''}e^{-i\Delta t}, \quad N(m,m') = \frac{M(m,m',m''=m-m')}{2k_m^2\partial_\omega D(\omega,k_m)|_{\omega=i\omega_m}}, \\ &M(m;m',m'') = \sum_s\frac{q_s}{m_s}\omega_{ps}^2\int\partial_v\left[\frac{k_{m''}\partial_v F_{s0}^{(0)}}{v-\omega_{m'}/k_{m'}}\right]\frac{dv}{k_m v-\omega_m}, \quad k_m = k_{m'}+k_{m''}; \Delta = \omega_{m'}+\omega_{m''}-\omega_m. \end{aligned} \tag{A11}$$

This is the wave-wave coupling equation of TID. When $k\lambda_{De}\ll 1$, IAWs have weak dispersion, $\omega_m/k_m \approx \omega_{m'}/k_{m'}$, then $M(m;,m',m'')$ can be simplified as

$$M(m;m',m'') = \frac{k''}{k_m}\sum_s\frac{q_s}{m_s}\omega_{ps}^2\int\frac{\partial_v F_{s0}^{(0)}dv}{(v-\omega_m/k_m)^3}. \tag{A12}$$

With the definition of $D(\omega_m,k_m)$ in Eq. (14), the denominator in $N(m,m')$ can be reduced to $2k_m^2\partial_\omega D(\omega=\omega_m,k_m) = -\sum_s\frac{2\omega_{ps}^2}{k_m}\int dv\frac{\partial_v F_{s0}^{(0)}(v)}{(v-\omega_m/k_m)^2}$. Then the coupling coefficient can be reduced to

$$N(m,m') = \frac{k_{m'}}{2}\frac{\sum_s\frac{q_s}{m_s}\omega_{ps}^2\int\frac{\partial_v F_{s0}^{(0)}(v)}{(v-\omega_m/k_m)^3}dv}{\sum_s\omega_{ps}^2\int\frac{\partial_v F_{s0}^{(0)}(v)}{(v-\omega_m/k_m)^2}dv}. \tag{A13}$$

APPENDIX B: THE COUPLING EQUATION FOR INITIAL MAXWELLIAN DISTRIBUTION

By assuming the initial Maxwellian distribution, $F_{s0}^{(0)}(v) = \frac{1}{v_{s,T}\sqrt{2\pi}}\exp(-v^2/2v_{s,T}^2)$, the coupling coefficient can be further reduced to

$$\begin{aligned} M(m;m',m'') &= \frac{k''}{k_m}\sum_s\frac{q_s}{m_s}\omega_{ps}^2\int\frac{\partial_v F_{s0}^{(0)}dv}{(v-\omega_m/k_m)^3} = -\frac{k''}{k_m}\sum_s\frac{q_s}{m_s}\frac{\omega_{ps}^2}{\sqrt{2\pi}v_{s,T}^3}\int\frac{v\exp\left[-v^2/2v_{s,T}^2\right]dv}{(v-\omega_m/k_m)^3} \\ &= -\frac{k''}{k_m}\sum_s\frac{q_s}{m_s}\frac{\omega_{ps}^2}{2v_{s,T}^4}\partial_{b_s}^2\,\mathrm{W}(b_s) = -\frac{k''}{k_m}\sum_s\frac{q_s}{m_s}\frac{\omega_{ps}^2}{2v_{s,T}^4}\left[\left(b_s{}^2-3\right)\mathrm{W}(b_s)+1\right] \end{aligned} \tag{B1}$$

where $b_s \equiv \omega_m/k_m/v_{s,T}$ is the ratio of phase velocity to thermal velocity of species s. The following relation: $\partial_b^2 \mathrm{W}(b) = (b^2 - 3)\mathrm{W}(b) + 1$ is used in the above equation, where $\mathrm{W}(b) = \frac{1}{\sqrt{2\pi}} \int_{-\infty}^{+\infty} \frac{xe^{-x^2/2}dx}{x-b} = 1 + (b/\sqrt{2})Z(b/\sqrt{2})$. With the definition of $D(\omega_m, k_m)$ in Eq. (14), the denominator in $N(m, m')$ can be reduced to

$$
\begin{aligned}
2k_m^2 \partial_\omega D(\omega, k_m)\big|_{\omega=\omega_m} &= \frac{-2}{k_m\sqrt{2\pi}} \sum_s \frac{\omega_{ps}^2}{v_{s,T}^3} \int \frac{v \exp\left(-v^2/2v_{s,T}^2\right)}{(v - \omega_m/k_m)^2} dv \\
&= \frac{-2}{k_m} \sum_s \frac{\omega_{ps}^2}{v_{s,T}^3} \partial_{b_s} \mathrm{W}(b_s) = \frac{2}{k_m} \sum_s \frac{\omega_{ps}^2}{v_{s,T}^3} ([1 - \mathrm{W}(b_s)]/b_s + b_s \mathrm{W}(b_s)),
\end{aligned} \tag{B2}
$$

where $-([(1 - W(b)]/b + bW(b))$ is used to get the above equation. Finally, we can obtain the coupling equations for the case of detuning $\Delta_{m,m'}/\omega_m \ll 1$ and $k_m \lambda_{De} \ll 1$ for the initial Maxwellian distribution:

$$
\begin{aligned}
\frac{d}{dt}\varphi_m &= -i \sum_{m'} N(m, m') \varphi_{m'} \varphi_{m''} e^{-i\Delta t}, \\
N(m, m') &= \frac{\frac{k_{m''}}{4} \sum_s \frac{q_s}{m_s} \frac{\omega_{ps}^2}{v_{s,T}^4} \left[\left(b_s{}^2 - 3\right)\mathrm{W}(b_s) + 1\right]|_{b_s=\omega_m/v_T k_m}}{\sum_s \frac{\omega_{ps}^2}{v_{s,T}^3} ([1 - \mathrm{W}(b_s)]/b_s + b_s \mathrm{W}(b_s))}, \\
k_m &= k_{m'} + k_{m''}; \Delta = \omega_{m'} + \omega_{m''} - \omega_m.
\end{aligned} \tag{B3}
$$

[1] V. T. Tikhonchuk, T. Gong, N. Jourdain, O. Renner, F. P. Condamine, K. Q. Pan, W. Nazarov, L. Hudec, J. Limpouch, R. Liska, M. Krůs, F. Wang, D. Yang, S. W. Li, Z. C. Li, Z. Y. Guan, Y. G. Liu, T. Xu, X. S. Peng, X. M. Liu *et al.*, Matter Radiat. Extremes **6**, 025902 (2021).

[2] H. H. Ma, X. F. Li, S. M. Weng, S. H. Yew, S. Kawata, P. Gibbon, Z. M. Sheng, and J. Zhang, Matter Radiat. Extremes **6**, 055902 (2021).

[3] M. Porkolab and R. P. H. Chang, Rev. Mod. Phys. **50**, 745 (1978).

[4] R. N. Franklin, Rep. Prog. Phys. **40**, 1369 (1977).

[5] F. Anderegg, M. Affolter, A. Ashourvan, D. H. E. Dubin, F. Valentini, and C. F. Driscoll, AIP Conf. Proc. **1668**, 020001 (2015).

[6] F. Valentini, T. O'Neil, and D. Dubin, Commun. Nonlinear Sci. Numer Simul. **13**, 215 (2008), Vlasovia 2006: The Second International Workshop on the Theory and Applications of the Vlasov Equation.

[7] A. Ashourvan, Ph.D. thesis, University of California, San Diego, 2014.

[8] D. H. E. Dubin, Phys. Rev. Lett. **121**, 015001 (2018).

[9] M. Affolter, F. Anderegg, D. H. E. Dubin, F. Valentini, and C. F. Driscoll, Phys. Rev. Lett. **121**, 235004 (2018).

[10] M. Affolter, F. Anderegg, D. H. E. Dubin, F. Valentini, and C. F. Driscoll, Phys. Plasmas **26**, 122108 (2019).

[11] D. H. E. Dubin, Phys. Plasmas **26**, 102113 (2019).

[12] S. H. Glenzer, L. M. Divol, R. L. Berger, C. Geddes, R. K. Kirkwood, J. D. Moody, E. A. Williams, and P. E. Young, Phys. Rev. Lett. **86**, 2565 (2001).

[13] C. Niemann, S. H. Glenzer, J. Knight, L. Divol, E. A. Williams, G. Gregori, B. I. Cohen, C. Constantin, D. H. Froula, D. S. Montgomery, and R. P. Johnson, Phys. Rev. Lett. **93**, 045004 (2004).

[14] H. C. Bandulet, C. Labaune, K. Lewis, and S. Depierreux, Phys. Rev. Lett. **93**, 035002 (2004).

[15] T. Chapman, B. J. Winjum, S. Brunner, R. L. Berger, and J. W. Banks, Phys. Plasmas **22**, 092116 (2015).

[16] B. J. Albright, L. Yin, K. J. Bowers, and B. Bergen, Phys. Plasmas **23**, 032703 (2016).

[17] T. Chapman, S. Brunner, J. W. Banks, R. L. Berger, B. I. Cohen, and E. A. Williams, Phys. Plasmas **21**, 042107 (2014).

[18] D. J. Liu, Q. Wang, T. Yang, R. J. Cheng, X. M. Li, X. X. Li, S. T. Zhang, S. Y. Lv, Z. M. Huang, Q. Wang, Z. J. Liu, L. H. Cao, and C. Y. Zheng, Plasma Phys. Controlled Fusion **65**, 055008 (2023).

[19] T. Chapman, R. L. Berger, B. I. Cohen, J. W. Banks, and S. Brunner, Phys. Rev. Lett. **119**, 055002 (2017).

[20] C. Riconda, A. Heron, D. Pesme, S. Hüller, V. T. Tikhonchuk, and F. Detering, Phys. Rev. Lett. **94**, 055003 (2005).

[21] C. Riconda, A. Heron, D. Pesme, S. Huller, V. T. Tikhonchuk, and F. Detering, Phys. Plasmas **12**, 112308 (2005).

[22] D. Pesme, C. Riconda, and V. T. Tikhonchuk, Phys. Plasmas **12**, 092101 (2005); **16**, 089903 (2009).

[23] B. I. Cohen, E. A. Williams, R. L. Berger, D. Pesme, and C. Riconda, Phys. Plasmas **16**, 032701 (2009).

[24] S. J. Karttunen, J. N. McMullin, and A. A. Offenberger, Phys. Fluids **24**, 447 (1981).

[25] S. Karttunen and R. Salomaa, Phys. Lett. A **72**, 336 (1979).

[26] H. Iwakura and M. Kono, J. Phys. Soc. Jpn. **43**, 2056 (1977).

[27] P. Michel, *Introduction to Laser-Plasma Interactions* (Springer International Publishing, New York, 2023), pp. 371–405.

[28] Z. J. Guo, H. B. Zhuo, H. L. Fan, M. Q. Li, S. Z. Wu, T. W. Huang, H. Zhang, and C. T. Zhou, Phys. Plasmas **30** (2023)

[29] C. Kuehn, *Multiple Time Scale Dynamics* (Springer, New York, 2015), Vol. 191.

[30] Q. S. Feng, C. Y. Zheng, Z. J. Liu, C. Z. Xiao, Q. Wang, and X. T. He, Phys. Plasmas **23**, 082106 (2016).
[31] R. L. Berger, S. Brunner, J. W. Banks, B. I. Cohen, and B. J. Winjum, Phys. Plasmas **22**, 055703 (2015).
[32] V. Pierrard and M. Lazar, Sol. Phys. **267**, 153 (2010).
[33] A. B. Langdon, Phys. Rev. Lett. **44**, 575 (1980).
[34] J. Qiu, L. Hao, L. Cao, and S. Zou, Nucl. Fusion **62**, 126072 (2022).
[35] J. Qiu, L. Hao, L. Cao, and S. Zou, Plasma Phys. Controlled Fusion **63**, 125021 (2021).
[36] J. P. Matte, M. Lamoureux, C. Moller, R. Y. Yin, J. Delettrez, J. Virmont, and T. W. Johnston, Plasma Phys. Controlled Fusion **30**, 1665 (1988).
[37] J. Zheng, C. X. Yu, and Z. J. Zheng, Phys. Plasmas **4**, 2736 (1997).
[38] H.-S. Xie, Phys. Plasmas **20**, 092125 (2013).
[39] R. Guo, Front. Astron. Space Sci. **9** (2022).
[40] T. Yang, Q. S. Feng, Y. X. Wang, Y. Z. Zhou, S. S. Ban, S. T. Zhang, R. Xie, Y. Jiang, L. H. Cao, Z. J. Liu, and C. Y. Zheng, Plasma Phys. Controlled Fusion **62**, 095009 (2020).
[41] Q. S. Feng, C. Z. Xiao, Q. Wang, C. Y. Zheng, Z. J. Liu, L. H. Cao, and X. T. He, Phys. Rev. E **94**, 023205 (2016).
[42] Y. X. Wang, Q. S. Feng, H. C. Zhang, Q. Wang, C. Y. Zheng, Z. J. Liu, and X. T. He, Phys. Plasmas **24**, 103122 (2017).
[43] Y. X. Wang, Q. Wang, C. Y. Zheng, Z. J. Liu, C. S. Liu, and X. T. He, Phys. Plasmas **25**, 100702 (2018).
[44] Z. J. Liu, X. T. He, C. Y. Zheng, and Y. G. Wang, Phys. Plasmas **16**, 093108 (2009).
[45] Z. J. Liu, S. p. Zhu, L. H. Cao, C. Y. Zheng, X. T. He, and Y. Wang, Phys. Plasmas **16**, 112703 (2009).
[46] F. Valentini, T. M. O'Neil, and D. H. E. Dubin, Phys. Plasmas **13**, 052303 (2006).
[47] F. Valentini, P. Trávníçek, F. Califano, P. Hellinger, and A. Mangeney, J. Comput. Phys. **225**, 753 (2007).
[48] A. Mangeney, F. Califano, C. Cavazzoni, and P. Travnicek, J. Comput. Phys. **179**, 495 (2002).
[49] S. K. Pandey and R. Ganesh, Phys. Scr. **96**, 125616 (2021).
[50] S. K. Pandey and R. Ganesh, Phys. Scr. **96**, 125615 (2021).
[51] M. Shoucri, Laser Part. Beams **35**, 706 (2017).
[52] G. Floquet, Ann. Sci. École Norm. Sup. **12**, 47 (1883).
[53] T. Chapman, R. L. Berger, S. Brunner, and E. A. Williams, Phys. Rev. Lett. **110**, 195004 (2013).
[54] D. Dubin and A. Ashourvan, Phys. Plasmas **22**, 102102 (2015).